ACS APPLIED MATERIALS & INTERFACES

Letter

www.acsami.org

Synchronous Electrosynthesis of Poly(xanthurenic acid)-Reduced Graphene Oxide Nanocomposite for Highly Sensitive Impedimetric Detection of DNA

Tao Yang, Qianhe Li, Le Meng, Xiaohong Wang, Wenwen Chen, and Kui Jiao*

State Key Laboratory Base of Eco-chemical Engineering, College of Chemistry and Molecular Engineering, Qingdao University of Science and Technology, Qingdao 266042, China

Supporting Information

ABSTRACT: A novel and simple synchronous electrochemical synthesis of poly(xanthurenic acid, Xa), electrochemically reduced graphene oxide nanocomposite (PXa-ERGNO), via cyclic voltammetry (CV) was reported, where graphene oxide (GNO) and Xa monomer were adopted as precursors. The resulting PXa-ERGNO nanocomposite was characterized by scanning electron microscopy, Fourier transform infrared spectroscopy, CV and electrochemical impedance spectroscopy (EIS). The $\pi-\pi^*$ interactions between the conjugated GNO layers and aromatic ring of Xa-enhanced the electropolymerization efficiency accompanied with an increased electrochemical response of PXa. The rich carboxyl groups of PXa-ERGNO film were applied to stably immobilize the probe DNA with amino groups at 5′ end via covalent bonding. The captured probe could sensitively and selectively recognize its target DNA via EIS. The dynamic detection range was from 1.0×10^{-14} mol/L to 1.0×10^{-8} mol/L with a detection limit of 4.2×10^{-15} mol/L due to the synergistic effect of integrated PXa-ERGNO nanocomposite. This graphene-based electrochemical platform showed intrinsic advantage, such as simplicity, good stability, and high sensitivity, which could serve as an ideal platform for the biosensing field.

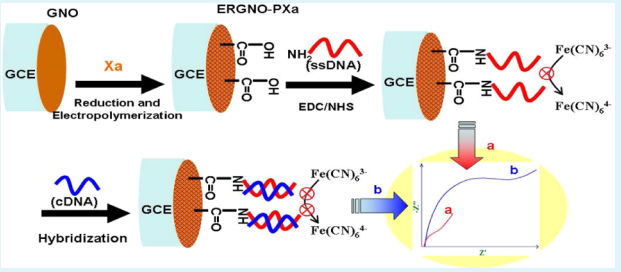

KEYWORDS: *graphene oxide, synchronous electrosynthesis, poly(xanthurenic acid), electrochemical reduction, impedimetric detection, synergistic effect*

Conducting polymers have been widely adopted for fabricating various electrochemical devices in many fields, such as sensors, supercapacitors, and electrocatalysts. To extend the functions and improve the performances of these devices, researchers frequently integrate conducting polymers with other functional materials to form composites and interfaces.[1−3] As a single-atom-thick carbon material with large surface area and high conductivity,[4,5] graphene has been employed as a matrix to disperse or embed conducting polymers for fabricating graphene−polymer hybrid electrodes in the fields of biosensors and electrocatalysts.[6−8] Among the synthetical methods of graphene−polymer hybrids, the electropolymerization route, due to its easy controlling the film property,[9] has been adopted. Additionally, it is convenient for next-step electrochemical applications and research. Typically, the electropolymerization route is performed normally by a stepwise process: (1) reduction of drop-casting graphene oxide (GNO), which was obtained from ultrasonication of graphite oxide (GO) solution; (2) electropolymerization at previously obtained reduced graphene oxide (RGNO)-modified electrode in a solution containing monomer, where RGNO acts as an ideal platform for designing composite nanomaterials served as high-performance electrocatalytic or electrochemical devices, etc.[10,11] For example, Mu performed electrocatalytic oxidative polymerization of *o*-phenylenediamine on a RGNO modified glassy carbon electrode (GCE). The obtained poly(*o*-phenylenediamine) showed expanded electrochemical activity in comparison with conventional poly(*o*-phenylenediamine) reported previously.[12]

It should be noted that a one-step electrochemical method for constructing conducting polymer and graphene composites has emerged as a green and fast approach with in situ precise control. At present, one-step synthesis of graphene-polymer hybrid film has been popular, where RGNO and the polymer were synchronously obtained. Feng et al. achieved one-step electrochemical synthesis of graphene/polyaniline composite film using GO and aniline monomer as the starting materials, the aniline monomer can be electropolymerized at anodic potential; meanwhile, the exfoliated GO precursor can be electrochemically reduced at cathodic potential.[13] The graphene/polyaniline composite film presented the large specific area, high conductivity, good biocompatibility, and fast redox properties. Horseradish peroxidase was entrapped into the film-modified electrode and applied to detect H_2O_2.

Received: January 28, 2013
Accepted: April 22, 2013
Published: April 22, 2013

In this work, GNO as the starting material was electrochemically reduced to ERGNO and the electropolymerization of xanthurenic acid (PXa) was achieved at anodic potential, simultaneously. The $\pi-\pi^*$ interactions between the conjugated GNO layers and aromatic rings monomer (xanthurenic acid, Xa) enhanced the electropolymerization efficiency, the film-forming ability and the water resistance of PXa-ERGNO. The rich carboxyl groups of PXa-ERGNO film can be adopted to covalently immobilize the probe ssDNA with the amino groups at 5′ end. The sensing platform could sensitively recognize its target DNA via electrochemical impedance spectroscopy (EIS) using $[Fe(CN)_6]^{3-/4-}$ as a classical indicator (Scheme 1). The simultaneously obtained PXa-ERGNO will be helpful for extending the application of graphene-based nanocomposite in the biosensing and electrochemical capacitors field.

Scheme 1. Schematic of Synchronous Electrosynthesis of PXa-ERGNO for DNA EIS Detection

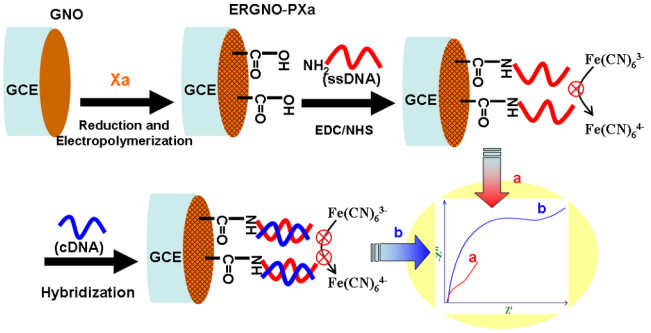

Here, the PXa-ERGNO composite film was synthesized via a facile one-step method (cyclic voltammetry, CV).[13] First, a homogeneous dispersion of GNO was dropped onto the surface of GCE and dried ready for electrosynthesis. Then, according to the initial report,[14] the electropolymerization of Xa was accomplished with CV range between 1.0 V and −0.5 V, and the electrochemical reduction of GNO via CV with a potential range from −0.2 V to −1.6 V.[15,16] So, various potential ranges were investigated to study the electrochemical process of PXa-ERGNO/GCE, which were shown in Figure 1A−C.

Figure 1A showed the electropolymerization of PXa in the range of 0.65 V to −0.60 V with a starting potential of 0.0 V. A sharp oxidation peak occurred at about 0.5 V (peak a), which indicates Xa oxidation, and triggered the electropolymerization of Xa. Evidence for the formation of the PXa was that a quasi-reversible redox process (peak b and c) appeared and increased during subsequent cycles,[14] revealing the electroactive film. The peak currents of b and c increased and reached stable-state at fifth cycle, illustrating that the PXa-GNO film on the modified electrode reached saturation.

As shown in Figure 1B, in the range of −0.2 V to −1.7 V, only the characteristic reduction peak of GNO appeared at nearly approximate −1.5 V (peak d) and then decreased obviously in the successive cycles, consistent with our previous report.[17]

When potential range was expanded (0.65 V to −1.7 V, Figure 1C), the characteristic peaks of electropolymerization of PXa (peaks a, b, and c) and electrochemical reduction of GNO (peak d) all appeared, showing the electropolymerization of PXa and the electrochemical reduction of GNO were realized in one step. It should be noted that characteristic peak currents

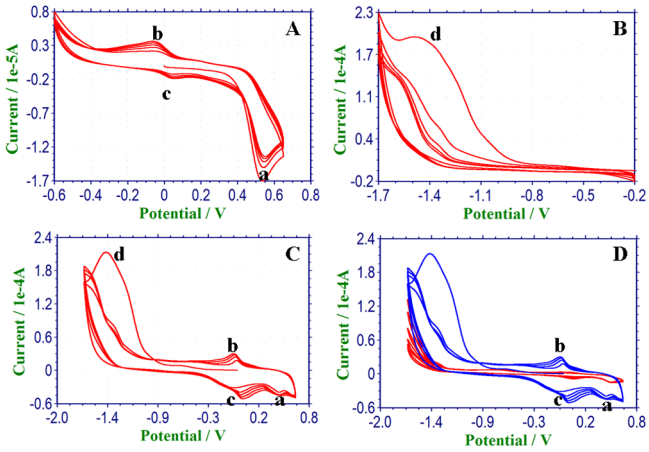

Figure 1. Comparison of CVs of the GNO/GCE in 0.3 mol/L PBS (pH 5.5) containing 4×10^{-4} mol/L Xa in different potential ranges: (A) 0.65 to −0.6 V; (B) −0.2 to −1.7 V; (C) 0.65 to −1.7 V. (D) CV of electrochemical synthesis of PXa/GCE (red line) and PXa-ERGNO/GCE (blue line).

of PXa (peaks a, b, and c) were higher compared to those in Figure 1A. The above results indicated that the electrochemical behavior of the resulting PXa was obviously affected by the potential range.

To further investigate the influence of GNO on electrochemical synthesis, the comparison of the electropolymerization of PXa on the bare GCE and GNO/GCE was displayed in Figure 1D. It can be seen that the specific oxidation peak (peak a) and quasi-reversible redox peak (peak b and c) of PXa-ERGNO/GCE (blue line) were larger than those of PXa/GCE (red line), which ascribed to existing of the GNO as precursor. Because of the $\pi-\pi^*$ interactions between the ERGNO layers and aromatic rings of Xa, graphene could serve as a strong adsorbing platform for Xa monomer[18] and promote the electropolymerization of PXa effectively.

Figure 2A showed a typical scanning electron microscopy (SEM) image of GNO with slight wrinkles.[19] After reduction, ERGNO (Figure 2B) showed a more corrugated and scrolled structure.[20] The resemblance of crumpled silk veil waves is intrinsic to graphene nanosheets.[21] However, PXa-ERGNO composite film (Figure 2C) illustrated a smoother and broader surface. The change of morphology demonstrated PXa-ERGNO composite film was synthesized successfully.

The reduction of GNO can be confirmed by X-ray photoelectron spectroscopy (XPS, see the Supporting Information, Figure S1), which reveals the presence of 93.6% atomic carbon, 3.94% atomic oxygen, 0.97% atomic nitrogen. The O/C ratio of ssDNA/PXa-ERGNO (4.2%) is much low.[22] The details, please see the Support Information. Those results indicate the considerable deoxygenation via the electrochemical reduction and the successful immobilization of DNA. The immobilization of DNA probes on the composite was also obviously identified by Fourier Transform infrared spectroscopy (FT-IR).[23] As shown in Figure 2D, the main peak at 1626 cm^{-1} can be assigned to the C═O stretching vibration of the amide bonds. It also illustrated bands appeared at 1584 cm^{-1} due to the combination of N−H bending and C−N stretching vibration of the amide bonds. From those specific peaks, the DNA probes were captured on the PXa-ERGNO composite by amide bond, which was formed between the amine groups at

dx.doi.org/10.1021/am400370s | ACS Appl. Mater. Interfaces 2013, 5, 3495−3499

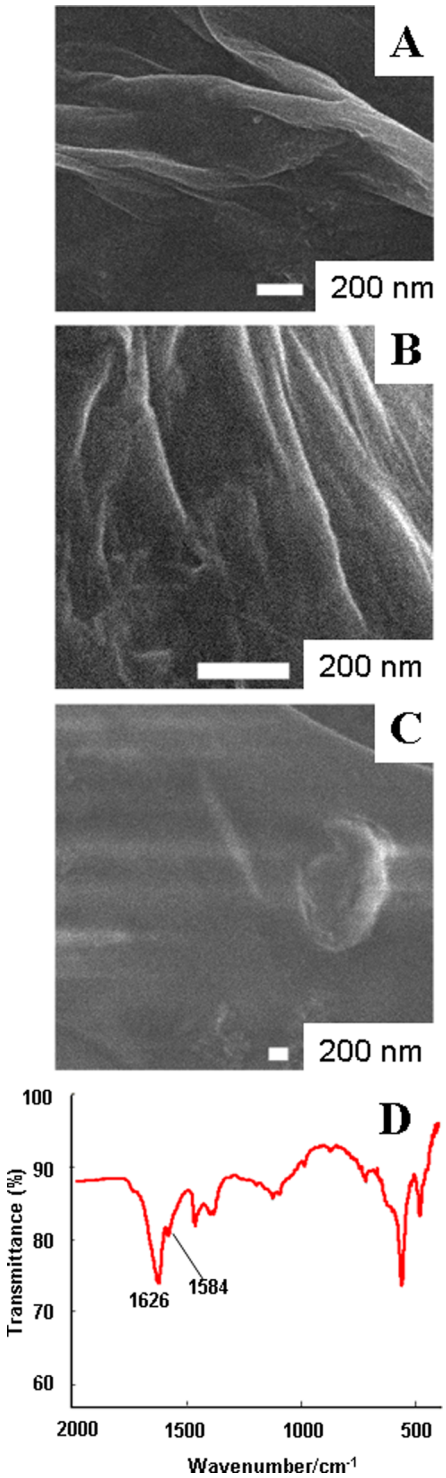

Figure 2. SEM images of (A) GNO, (B) ERGNO, and (C) PXa-ERGNO. (D) FT-IR spectrum of the ssDNA/PXa-ERGNO/GCE.

the ends of ssDNA and carboxyl groups of PXa with the activation of EDC/NHS.

The self-redox signals of PXa on the different modified electrodes were recorded by CV in 0.3 mol/L PBS (pH 7.0)[14] and shown in Figure S2A in the Supporting Information. The redox peak current of PXa-ERGNO/GCE (curve c) showed highest value as compared with bare GCE (curve a) and PXa/GCE (curve b), which indicated that the presence of ERGNO could dramatically enhance the electrochemical activity of PXa, being consistent with the result of Figure 1D.

The change of electropolymerization cycles could directly control the electrochemical activity of composite film. As shown in Figure S2B in the Supporting Information, the self-redox signal of PXa reached maximum when 5 cycles were adopted, and then decreased with further increase in cycle. Therefore, 5 cycles were selected to present the highest electrochemical signal.

EIS, as a sensitive and reliable tool, has been adopted in electrochemical biosensors to monitor the change of electrode interface based on biological and chemical molecule recognition.[24,25] Figure 3A displayed the representative Nyquist plots

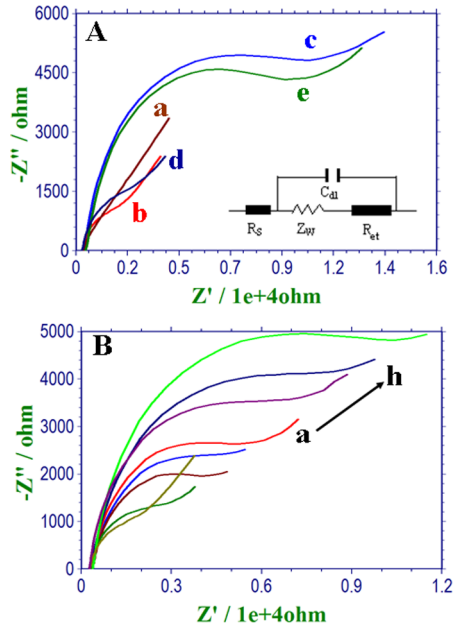

Figure 3. (A) Representative Nyquist diagrams of 1.0×10^{-3} mol/L $[Fe(CN)_6]^{3-/4-}$ recorded at (a) PXa-ERGNO/GCE, (b) ssDNA/PXa-ERGNO/GCE, (c) the electrode hybridized with cDNA, (d) the electrode hybridized with ncDNA, and (e) the electrode hybridized with single-base mismatched DNA. The inset is model electrical equivalent circuit to describe the data shown in the inset. (1) electrolyte resistance, R_s; (2) the lipid bilayer capacitance, C_{dl}; (3) charge transfer resistance, R_{et}; (4) Warburg impedance, Z_w. (B) Representative Nyquist diagrams recorded at the ssDNA/PXa-ERGNO/GCE (a) and after hybridization with different concentrations of the PML/RARA target sequence: (b) 1.0×10^{-14} mol/L to (h) 1.0×10^{-8} mol/L.

recorded at different electrodes in 0.1 mol/L NaCl containing 1.0×10^{-3} mol/L $[Fe(CN)_6]^{3-/4-}$(1:1). Distinct differences in the electron transfer resistances (R_{et}, which can be directly measured as the semicircle diameter of the Nyquist plots) were observed with the stepwise formation of the modified electrode. It could be seen that the PXa-ERGNO/GCE (curve a) showed nearly no arc as an almost straight line. Subsequently, after the NH_2-ssDNA was captured through covalent bonding (curve b), the R_{et} value increased, which indicated that the negative charge of NH_2-ssDNA inhibited redox probe $[Fe(CN)_6]^{3-/4-}$. After hybridization with target DNA, the resulting dsDNA owns more negative charge, repels the interfacial electron transfer and thus leads to an enhanced R_{et} value (curve c).

Meanwhile, the selectivity of the biosensor was also investigated. After hybridization with noncomplementary

dx.doi.org/10.1021/am400370s | ACS Appl. Mater. Interfaces 2013, 5, 3495−3499

sequence DNA (ncDNA, curve d), the change of the R_{et} value was negligible compared with curve b, showing that the hybridization hardly happens. Besides, single-base mismatched DNA (curve e) could be distinguished via comparing the change of the R_{et} value induced by complementary DNA (cDNA, curve c). The detail data analysis and histogram for comparison of signal change induced by hybridization with cDNA, ncDNA, and single-base mismatched DNA please see the Support Information, Figure S3. Note: Each point is the mean of three measurements, and the error bars correspond to the standard deviation. The results demonstrated that this DNA biosensor could be utilized for DNA selective recognition and detection.

Figure 3B showed the Nyquist diagrams obtained on the ssDNA/PXa-ERGNO/GCE and hybridization with different concentrations of the promyelocytic leukemia and retinoic acid receptor alpha (PML/RARA) target sequence. The difference of the R_{et} value (namely ΔR_{et}) between before and after hybridization was linear with the negative logarithm of the PML/RARA fragment concentrations. The dynamic detection range for the PML/RARA fragment was from 1.0×10^{-14} mol/L to 1.0×10^{-8} mol/L with the regression equation ΔR_{et} (kΩ) = 1.1663 lg C + 16.768 and the regression coefficient (γ) 0.9742 (please see the Supporting Information, Figure S4). A detection limit of this label-free impedance detection assay was 4.2×10^{-15} mol/L using 3σ (where σ was the standard deviation of the blank solution, n = 11). The comparison of sensitivity between EIS detection using $[Fe(CN)_6]^{3-/4-}$ and DPV using methylene blue (MB) and $[Fe(CN)_6]^{3-/4-}$ please see the Supporting Information, Figures S5−S7.

The performance of the proposed biosensor was compared with other DNA electrochemical biosensors for PML/RARA target sequence (see Table S1 in the Supporting Information). Because of adopting $[Fe(CN)_6]^{3-/4-}$ as signal probe, this DNA biosensor also had an outstanding detection limit and wide detection range for the target DNA assay.

The reproducibility of this DNA sensor was investigated by a parallel measurement method for a low concentration of target DNA sequence. Six parallel-made DNA sensors were used to detect a 1.0×10^{-10} mol/L target DNA sequence with a relative standard deviation (RSD) of 8.2%. The results indicated that the reproducibility of this DNA biosensor was satisfactory.

The stability of the DNA biosensor was also tested. The prepared ssDNA/PXa-ERGNO/GCE was incubated in ultrapure water, Tris-HCl solution (pH 7.0), and PBS (pH 7.0) at 25 °C for 3 h, respectively. The EIS results showed that the incubated electrode showed same behavior as compared with the unincubated electrode. Thus, the prepared DNA biosensor was suited as a stable detection platform.

In summary, we have electrochemically synthesized an integrated PXa-ERGNO hybrid in one-step process via a simple CV method, where GNO as the precursor was electrochemically reduced to ERGNO at cathodic potential; meanwhile, the electropolymerization of Xa was achieved at anodic potential. The electropolymerization efficiency and accompanied electrochemical activity of PXa was obviously enhanced due to the $\pi-\pi^*$ interactions between the conjugated GNO layers and aromatic rings of Xa. The rich carboxyl groups of PXa-ERGNO film could be adopted to covalently immobilize the probe ssDNA through the activation of EDC and NHS. The resulting sensing platform could sensitively recognize its target DNA. The dynamic detection range was from 1.0×10^{-14} mol/L to 1.0×10^{-8} mol/L with a detection limit of 4.2×10^{-15} mol/L because of the synergistic effect of integrated PXa-ERGNO nanocomposite.

■ ASSOCIATED CONTENT

Supporting Information

Detail of experiment including chemicals, instrumentations, and related experimental results. This material is available free of charge via the Internet at http://pubs.acs.org.

■ AUTHOR INFORMATION

Corresponding Author

*E-mail: kjiao@qust.edu.cn.

Notes

The authors declare no competing financial interest.

■ ACKNOWLEDGMENTS

This work was supported by the National Natural Science Foundation of China (21275084, 20975057, 20805025), Doctoral Foundation of the Ministry of Education of China (No. 20113719130001), Outstanding Adult-Young Scientific Research Encouraging Foundation of Shandong Province (BS2012CL013), and Scientific and Technical Development Project of Qingdao (12-1-4-3-(23)-jch).

■ REFERENCES

(1) Yoon, H.; Jang, J. *Adv. Funct. Mater.* **2009**, *19*, 1567−1576.
(2) Dhand, C.; Das, M.; Datta, M.; Malhotra, B. D. *Biosens. Bioelectron.* **2011**, *26*, 2811−2821.
(3) Hu, Y. W.; Yang, T.; Wang, X. X.; Jiao, K. *Chem.—Eur. J.* **2010**, *16*, 1992−1999.
(4) Chen, D.; Feng, H. B.; Li, J. H. *Chem. Rev.* **2012**, *112*, 6027−6053.
(5) Yan, L.; Zheng, Y. B.; Zhao, F.; Li, S. J.; Gao, X. F.; Xu, B. Q.; Weiss, P. S.; Zhao, Y. L. *Chem. Soc. Rev.* **2012**, *41*, 97−114.
(6) Al-Mashat, L.; Shin, K.; Kalantar-zadeh, K.; Plessis, J. D.; Han, S. H.; Kojima, R. W.; Kaner, R. B.; Li, D.; Gou, X. L.; Ippolito, S. J.; Wlodarski, W. *J. Phys. Chem. C* **2010**, *114*, 16168−16173.
(7) Yan, X. B.; Chen, J. T.; Yang, J.; Xue, Q. J.; Miele, P. *ACS Appl. Mater. Interfaces* **2010**, *2*, 2521−2529.
(8) Kim, G. H.; Hwang, D. H.; Woo, S. I. *Phys. Chem. Chem. Phys.* **2012**, *14*, 3530−3536.
(9) Cosnier, S.; Holzinger, M. *Chem. Soc. Rev.* **2011**, *40*, 2146−2156.
(10) Huang, X.; Qi, X. Y.; Boey, F.; Zhang, H. *Chem. Soc. Rev.* **2012**, *41*, 666−686.
(11) Yang, T.; Li, X.; Li, Q. H.; Guo, X. H.; Guan, Q.; Jiao, K. *Polym. Chem.* **2013**, *4*, 1228−1234.
(12) Mu, S. L. *Electrochim. Acta* **2011**, *56*, 3764−3772.
(13) Feng, X. M.; Li, R. M.; Ma, Y. W.; Chen, R. F.; Shi, N. E.; Fan, Q. L.; Huang, W. *Adv. Funct. Mater.* **2011**, *21*, 2989−2996.
(14) Silva, F. A. S.; Lopes, C. B.; Costa, E. O.; Lima, P. R.; Kubota, L. T.; Goulart, M. O. F. *Electrochem. Commun.* **2010**, *12*, 450−454.
(15) Du, M.; Yang, T.; Li, X.; Jiao, K. *Talanta* **2012**, *88*, 439−444.
(16) Gong, J. M.; Miao, X. J.; Wan, H. F.; Song, D. D. *Sens. Actuators, B* **2012**, *162*, 341−347.
(17) Du, M.; Yang, T.; Jiao, K. *J. Mater. Chem.* **2010**, *20*, 9253−9260.
(18) Liu, J. Q.; Tao, L.; Yang, W. R.; Li, D.; Boyer, C.; Wuhrer, R.; Braet, F.; Davis, P. T. *Langmuir* **2010**, *26*, 10086−10075.
(19) Zhou, M.; Wang, Y. L.; Zhai, Y. M.; Zhai, J. F.; Ren, W.; Wang, F.; Dong, S. J. *Chem.—Eur. J.* **2009**, *15*, 6116−6120.
(20) Yang, J.; Deng, S. Y.; Lei, J. P.; Ju, H. X.; Gunasekaran, S. *Biosens. Bioelectron.* **2011**, *29*, 159−166.
(21) Guo, H. L.; Wang, X. F.; Qian, Q. Y.; Wang, F. B.; Xia, X. H. *ACS Nano* **2009**, *3*, 2653−2659.
(22) Zhou, M.; Zhai, Y. M.; Dong, S. J. *Anal. Chem.* **2009**, *81*, 5603−5613.

(23) Zhang, W.; Yang, T.; Jiao, K. *Biosens. Bioelectron.* **2012**, *31*, 182−189.
(24) Yang, T.; Guan, Q.; Guo, X. H.; Meng, L.; Du, M.; Jiao, K. *Anal. Chem.* **2013**, *85*, 1358−1366.
(25) Yang, T.; Guan, Q.; Li, Q. H.; Meng, L.; Wang, L. L.; Liu, C. X.; Jiao, K. *J. Mater. Chem. B* **2013**, DOI: 10.1039/C3TB20171F.